Arabian Journal of Chemistry (2021) **14**, 103120

King Saud University

Arabian Journal of Chemistry

www.ksu.edu.sa
www.sciencedirect.com

ORIGINAL ARTICLE

Nanocomposite hydrogels for melanoma skin cancer care and treatment: *In-vitro* drug delivery, drug release kinetics and anti-cancer activities

Samina Nazir [a], Muhammad Umar Aslam Khan [b,c,d,*], Wafa Shamsan Al-Arjan [a], Saiful Izwan Abd Razak [c,e], Aneela Javed [f], Mohammed Rafiq Abdul Kadir [c]

[a] *Department of Chemistry, College of Science, King Faisal University, P.O. Box 400, Al-Ahsa 31982, Saudi Arabia*
[b] *Department of Polymer Engineering and Technology, University of the Punjab, Lahore, Pakistan*
[c] *BioInspired Device and Tissue Engineering Research Group, School of Biomedical Engineering and Health Sciences, Faculty of Engineering, Universiti Teknologi Malaysia, 81300 Skudai, Johor, Malaysia*
[d] *School of Biomedical Engineering, Med-X Research Institute, Shanghai Jiao Tong University (SJTU), 1954 Huashan Road, Shanghai 200030, China*
[e] *Centre for Advanced Composite Materials, Universiti Teknologi Malaysia, Skudai, Johor, Malaysia*
[f] *Department of Healthcare Biotechnology, Atta ur Rahman School of Applied Biosciences, National University of Sciences and Technology, Islamabad, Pakistan*

Received 18 January 2021; accepted 8 March 2021
Available online 26 March 2021

KEYWORDS

Biopolymers;
Reduce graphene oxide;
Macromolecules;
Smart nanomedicine;
Melanoma skin cancer;
In-vitro drug delivery

Abstract Malignant melanoma is a lethal human skin cancer that is not easily treatable through traditional medicines, surgeries, and therapies. Millions of cases are recorded annually to cure physiological skin defects by chemotherapy that causes several adverse effects and challenges. Moreover, pathogenic infections might aggravate infection with subsequent ulceration or cutaneous melanoma. Accordingly, we synthesized nanodrug by loading chemotherapeutic agent, Fluorouracil (5FU), onto the reduced graphene oxide (rGO). We then extracted arabinoxylan (ARX) from the husk of *Plantago Ovata* and functionalized it into carboxymethylarabinoxylan (CMARX) and loaded synthesized nanodrug. We have crosslinked CMARX/nanodrug with different amount of tetraethylorthosilicate (TEOS) to prepare nanocomposite hydrogel rGO-5FU-CMARX system for melanoma skin cancer care and treatment. These nanocomposite hydrogel systems rGO-5FU-CMARX have exhibited different physicochemical properties. These properties were analyzed through FTIR, SEM, water contact angle, swelling in different media (aqueous and

* Corresponding author at: BioInspired Device and Tissue Engineering Research Group, School of Biomedical Engineering and Health Sciences, Faculty of Engineering, Universiti Teknologi Malaysia, 81300 Skudai, Johor, Malaysia.
E-mail address: umar007khan@gmail.com (M. Umar Aslam Khan).
Peer review under responsibility of King Saud University.

Production and hosting by Elsevier

https://doi.org/10.1016/j.arabjc.2021.103120

PBS) and biodegradation in PBS media. The *in-vitro* activities, i.e., drug delivery via Franz diffusion, antibacterial against *S. aureus* and *P. aeruginosa* and the anticancer activities was performed against Uppsala 87 Malignant Glioma (*U-87*) cell lines. Moreover, rGO-5FU-CMARX nanocomposite hydrogels displayed different antimicrobial and anticancer activities based on different crosslinking. Hence, an inventive rGO-5FU-CMARX based nanocomposite hydrogel drug-delivery system was developed to treat malignant melanoma skin cancer after bacterial infections.

1. Introduction

The skin is a vital organ in our bodies, with incredible regeneration capabilities. However, skin tissues are delicate and prone to melanoma skin cancer. Skin cancer is a common and challenging type of cancer that affects one out of every five Americans once in their lives (Gordon, 2013). Melanoma is an aggressive form of cancer that is relatively common but has a poor prognosis. It is the metastatic stage of cancer, as evidenced by increased tumor cell invasion and cancer migration to specific organs (Uddin et al., 2015). Furthermore, pathogenic infections acquired as a result of a relatively weak immune system exacerbate this complicated situation. Such infections exacerbate the complexity of carcinogenesis and increase patient mortality (Schaible and Stefan, 2007). As a result, recent research reports regarding the development of capable Drug Delivery Systems (DDS), particularly polymeric systems leading to the controlled delivery of chemotherapeutics, show an increasing effort (Shah et al., 2016; Uddin et al., 2020). Nanotechnology has only recently emerged in the last two decades. Still, it has already provided considerable opportunities to address the limitations of traditional DDS mechanisms, as well as for biotechnology, biomedicine, and other fields. Nanocarriers with the appropriate characteristics can effectively target and release drugs at the desired location (Dong et al., 2019). Nanoparticle multifunctional features have enabled substantial shifts in the drug delivery sector in the current scenario. Their nano-size design has a multifunctional surface and enhanced loaded biochemical impact of bio-actives molecules. The sustained release of DOX from these nanocarriers at the target site has been observed (Misra and Sahoo, 2010).

Graphene nanocomposites have unique properties, such as a larger surface area for therapeutic loading agents for targeted delivery. Therapeutic agents are loaded due to π-π ring stacking and wetting behavior. Composite hydrogels can be created by dispersing graphene-based nanomaterials uniformly in polymeric media (Karimi et al., 2016). Hydrogels resolve to treat skin cancer by releasing drugs in a controlled and targeted manner under many physiological conditions. Different polymers (both synthetic and natural) can be used to make hydrogel to treat skin problems. Natural polymers could be an excellent alternative option for biodegradation, biocompatibility, cytocompatibility, and long-term release. These therapeutic agents were released when they degraded or swelled under various physicochemical conditions (i.e., pH, temperature and concentrations, etc.) (Thambi et al., 2017). Hydrogels made from carboxymethyl cellulose, chitosan, bovine serum albumin, and other biopolymers were widely considered for drug delivery systems (Khan et al., 2019; Khan et al., 2020). A potential natural polymeric system in biomedical applications is a carboxymethyl-based polysaccharide derivative with multifunctional properties such as pH responsiveness, chemical reactivity, water solubility, and biodegradability (Moscovici, 2015).

We have developed novel nanocomposite hydrogels rGO-5FU-CMARX, containing carboxymethylarabinoxylan and fluorouracil loaded graphene oxide, as novel nanocarriers to treat melanoma skin cancer. The synthesized hydrogels' physicochemical properties have been analyzed using Fourier-transform infrared (FTIR), scanning electron microscope (SEM), water contact angle (WCA), and *in-vitro* biodegradation and swelling assay. The anticancer activity of these nanocomposite hydrogels was tested against *U-87* cell lines. The Franz diffusion cell method was used to determine the *in-vitro* drug release of Fluorouracil. Fluorouracil is a well-known anticancer drug used to treat skin cancer. The surface area of rGO offers a substantial amount of drug loading and release under photothermal phenomena. Under humidity and thermal agitation, the developed nanocomposite hydrogels could produce a sustainable release of drug payloads. The prepared nanocomposite hydrogels proved to be potential biomaterials for skin cancer treatment and care from the results. These nanocomposite hydrogels are usable in a clinical setting to treat and heal skin cancer and consequential infections.

2. Materials and methods

2.1. Materials

The seed husk of *Plantago ovata* was purchased from a local market of Johor Bahru, Malaysia, and ARX was extracted using a previously reported method (Saghir et al., 2008). The graphene sheets were purchased from Sigma Aldrich, and rGO was synthesized by the well-reported protocol (Deb and Vimala, 2018). Sigma Aldrich supplied chitosan (CS), Tripolyphosphate (TPP), Tetraethyl orthosilicate (TEOS), tripolyphosphate (TPP), phosphate buffer saline solution (PBS), acetic acid, sodium monochloroacetate ($ClCH_2COONa$), and sodium hydroxide (NaOH). Fisher Scientific supplied the membrane filter papers (pore size, 0.45 μm). Fetal bovine serum (FBS) was supplied by Gibco BRL (New York, USA). Dulbecco's Modified Eagle Medium (DMEM) was purchased from Mediatech Inc. (Herndon, VA, USA). The cell line *U-87* MG (abbreviation for Uppsala 87 Malignant Glioma) is commonly used in cancer research. These cell lines were kindly provided by the signaling and membrane ion transport Laboratory, Universitè de Poitiers.

2.2. Synthesis of sodium carboxymethylarabinoxylan (CMARX)

Arabinoxylan was extracted using blond psyllium seed husk, using a reported procedure with little modification (Saghir et al., 2008). The seecd husk of *Plantago ovata* (500 g) was immersed in 3 L of deionized water for 24 h. It was blended with NaOH soln. (2.5%) to regulate pH with magnetic stirring for 5 min. The insoluble component of the seed husk has been separated by vacuum filtration from the gel. The gel was coagulated using concentrated acetic acid and neutralized through washing with deionized water. The obtained gel was lyophilized to get dried arabinoxylan powder (ARX). Afterward, a reported procedure was used to synthesize the carboxymethyl arabinoxylan (CMARX) with little alterations (Saghir et al., 2008). ARX (2 g) was dispersed into ethanol with continuous stirring for 1 h at ambient temperature. Then, $ClCH_2COONa$ and NaOH soln. (25%) were added to ARX at 55 °C for 5 h. Then a water/methanol mixture (80%, v/v) was added. The obtained CMARX was neutralized using acetic acid, washed using ethanol, and was dried in a vacuum to get a fine powder of CMARX.

2.3. Synthesis of nanodrug

The nanodrug was synthesized by loading a solution of 5FU (1 mg/ml) into rGO through a simple incubation for 24 h, while chitosan (0.1%, w/v) was coated via a solvent gelation method (Zhao et al., 2018). Sodium tripolyphosphate (0.125%, w/v) was used to crosslink chitosan and stabilize the prepared nanocomposites. These prepared nanocarriers were centrifuged (15,000 for 30 min), freeze-dried, and treated with lactose monohydrate (2%, w/v) as cryo-protectant and whole process has summerized in Figure Scheme 1.The model drug (5FU) stirred for 24 h and later for 48 h with the rGO with a final concentration of 1 mg/mL. It was observed that after 24 and 48 h, the loading efficiency of 5FU was 45.15 ± 1.79% and 57.37 ± 2.54%, respectively. The fine powder of freeze-dried nanocarriers was packed into an airtight vessel to formulate later nanocomposite hydrogels for skin cancer melanoma care and treatment.

2.4. Fabrication of nanocomposite hydrogels

The nanocomposite hydrogels were fabricated by the simple blending method. Briefly, 1.5 g of ARX powder was dispersed into deionized water and stirred with a hybrid nanodrug (rGO-5FU, 20 mg) to have a homogenized suspension. TEOS was added dropwise as a crosslinker with the different amounts (50, 100, 150, and 200 µm) into suspension under continuous stirring for 30 min at ambient conditions for furnish rGO-5FU-CMARX. These nanocomposite hydrogels were fabricated with different amount of crosslinker to study the best formulation for malignant melanoma skin cancer care and treatment. A 10 mL of nanocomposite hydrogels suspension was poured into Petri dishes from each formulation and was dried for 24 h at 55 °C. Nanocomposite hydrogel samples obtained were referred to as "NCH-1, NCH-2, NCH-3, and NCH-4," containing 50, 100, 150, and 200 µm TEOS. The whole process has been summarised in Figure Scheme 2.

3. Characterizations

3.1. FTIR analysis

The well-dried nanocomposite hydrogels were analyzed through FTIR spectroscopy (Nicolet 5700, Waltham, MA, USA) for functional group analysis. The range of FTIR was kept from 4000 to 400 cm^{-1} with 150 scans.

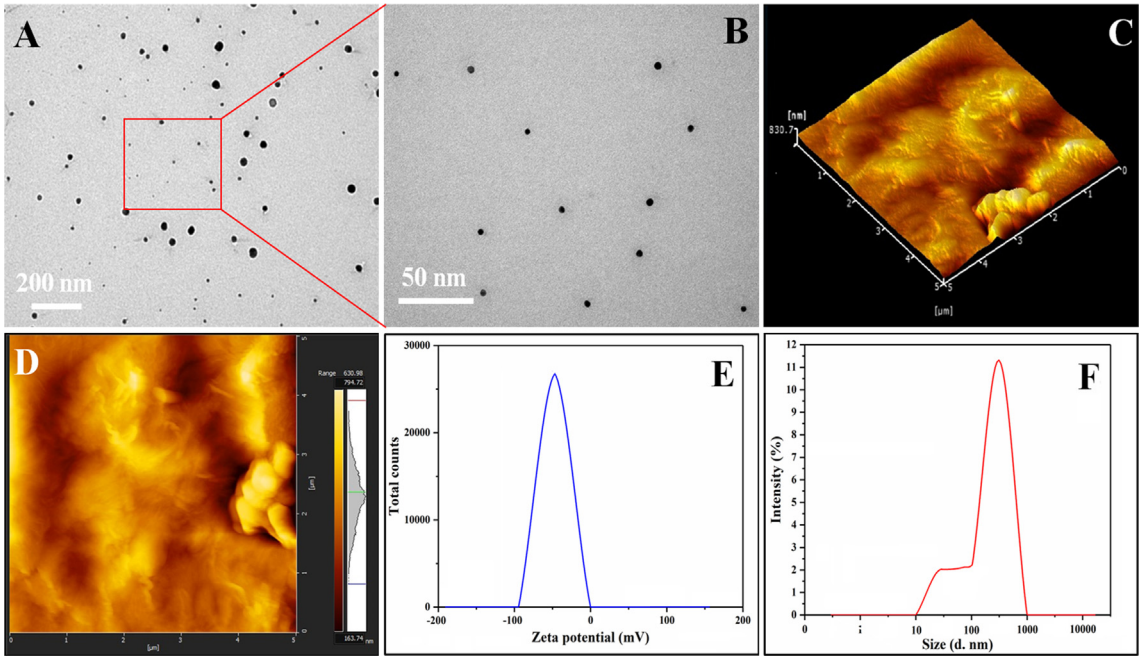

Fig. 1 Presents the microstructure analysis of the nano-drug. (A & B) TEM analysis with different scale, (C, D) three-dimensional (3D) and two-dimensional (2D) surface topography of nano-drug. (E, F) zeta potential and hydrodynamic particle of nanodrug.

3.2. Wetting analysis

The wetting analysis (hydrophobicity and hydrophilicity) of nanocomposite hydrogels were analyzed through a JY-82 water contact angle meter (Chengde DingSheng testing system, China).

3.3. Microstructural morphology (SEM, AFM and TEM)

The nanocomposite hydrogels were dried well and gold-sputtered to determine the surface morphology using SEM (JSM-6701S). The well-dried film of nanocomposite hydrogels were prepared (1×1 cm^2) into a square shape. The surface topography was determined using Park System XE-100 atomic force microscopy system (Suwon, Korea). The CM-silicon probes, 512×512 pixel topography images were obtained in the air in contact mode (Park Systems, Korea). The nanostructural analysis of nanodrug was conducted using an HT7700 transmission electron microscope (Hitachi, Japan).

3.4. Swelling analysis

The swelling analysis of nanocomposite hydrogels was conducted to determine swelling behavior. The hydrogel samples (50 mg) were cut in square, and initial weight (W_i) was recorded. The nanocomposite hydrogels were soaked into different media (aqueous and PBS) with pH 6.7 at room temperature. These nanocomposite hydrogels were removed after a fixed interval of time. The extra media was removed using tissue paper carefully, and the final weight (W_f) was recorded for each sample. The percentage of swelling for all composite hydrogels was calculated through Eq. (1).

$$\text{Swelling}(\%) = \frac{W_f - W_i}{W_i} \times 100 \quad (1)$$

Whereas, $\boldsymbol{W_f}$ = final weight, $\boldsymbol{W_i}$ = initial weight.

3.5. Biodegradation

The biodegradation behavior of nanocomposite hydrogels was determined under standard *in-vitro* conditions. The nanocomposite hydrogels (35 mg) were sliced into a square shape. The nanocomposite hydrogels were placed into separate PBS solution (pH 7.4) and incubated at 37 °C under 5% CO_2 to observe the degradation at a different time (1, 2, 3, 5, and 7 days). The biodegradation analysis was conducted under perfect sterile conditions to control pathogen contamination. The biodegradation of nanocomposite hydrogels was assessed by weight loss, using Eq. 3.

$$\textit{Weight loss}\ (\%) = \frac{W_o - W_i}{W_o} \times 100 \quad (2)$$

Whereas $\boldsymbol{W_o}$ = final weight of nanocomposite hydrogels, $\boldsymbol{W_i}$ = initial weight of nanocomposite hydrogels.

3.6. In-vitro studies

3.6.1. Antibacterial activities

The nanocomposite hydrogels (NCH1-NCH4) were investigated for antibacterial activities against severe disease-causing pathogens (i.e., *S. aureus and P. aeruginosa*). A well-reported method by Valgas was used to study antibacterial activities (Valgas and Souza, 2007). Petri dishes were properly sterilized, filled with molten agar and let to solidify. The sterile glass rod was used to spread bacterial strains uniformly. Each nanocomposite hydrogel (60 μL) sample was placed over the Petri dish using a micropipette and incubated at 37 ℃ for 24 h. The bactericidal antibacterial activities were measured (mm) through CLSI disc diffusion breakpoints (Huang et al., 2014).

3.6.2. Anticancer activities

Anticancer activities were measured through indexing the mitochondrial activity of alive cells using MTT assay. Cancer *U87* cell lines were cultured at 37 °C for 24 h in DMEM supplemented with fetal bovine serum (10%) and Penicillin-Streptomycin solution (1%) under 5% CO_2 atmosphere. When the cultures achieved about 70% confluence, cells were counted, and 10,000 cells were plated in each well of a 96-well culture plate. The plate was incubated in a CO_2 incubator for 24 h. MTT (5 mg/ml) was dissolved in and added to test wells after 24 h of cells' growth with nanocompoite hydrogels. After adding MTT (15 μL/well), cells were incubated again at 37 °C. After 3 h, the supernatant was removed, and residues were dissolved in DMSO (150 μL/well). The plate was covered with foil to protect from light and immediately measured for the absorbance in Spectrophotometer-Plate reader at 550 nm wavelength. The experiment was performed in triplicates, and the results are the average of three experiments. The cell viability (%) was evaluated by Eq. (3).

Whereas abs_{sample} absorbance of sample, abs_{blank} absorbance of blank and $abs_{control}$ absorbance of control.

3.6.3. Cell morphology

The *U-87* cell lines were cultured, using DMEM Supplemented with 10% FBS and 1% Penicillin-Streptomycin solution, at 37 °C for 24 h. When the cultures achieved the desired confluence, 10,000 cells were plated in each well of a 96-well culture plate. The plate was incubated in a CO_2 incubator for 24 h. The nanocomposite hydrogels were then added to the wells. The cellular morphology was obtained by photographing the cells using the camera attached with the light microscope (Nikon Eclipse TS100). The pictures were taken at 10X magnification and maximum light exposure. The cells were photographed at three intervals, i.e., 24, 48 and 72 h after adding the hydrogels.

3.6.4. Franz diffusion drug delivery

The Franz diffusion cell was used with a slight modification to analyze delivery of 5FU from the nanocomposite hydrogels (Perme Gear Inc), as reported by Abba et al. (2019). In Franz diffusion cells, the receptor volume is ~ 7 mL and 1.767 cm^2 is diffusional. These nanocomposite hydrogel samples were cut in the appropriate size to fill in the donor compartment and placed at −20 °C. The tests were performed in triplicate, and permeation was determined by circular cellulose nitrate membrane (Whatman 7184-002). The temperature of the outer jacket was adjusted at 37 °C (Polystat) and thermostated. The inner compartment was filled with PBS at different pH (pH 6.4, 7.4 and 8.4) and stirred at 600 rpm using the magnetic stirring bar. The experiment was initiated by adding PBS

(100 µL) in the donor compartment and covered by Parafilm to maintain airtight (Trovatti et al., 2012). The whole analysis was conducted under similar conditions. The sample (1 mL) was taken from the receptor compartment and instantly replaced with fresh PBS (1 mL) at 37 °C. The sample (1 mL) from the receptor compartment was quantified through UV–Visible (HATCH D500), and the absorbance was measured at 266 nm (Thakur et al., 2008). The PBS buffer solution was used as a standard, and drug release kinetics were measured by graph calibration.

3.6.5. Drug release kinetics

The release kinetics of Fluorouracil drug was studied through six different mathematical models, i.e., zero-order, first-order, Higuchi, Korsmeyer-Peppas, Hixson-Crowell, and Baker-Lonsdale models. (Eqs. (4)–(9)) using in-vitro transdermal drug release data (Alkafajy and Albayati, 2020; Jahromi et al., 2020).

$$\textbf{Zero order} \qquad Mt = M_o + k_o t \tag{3}$$

$$\textbf{First order} \qquad logC_O - \frac{kt}{2.303} \tag{4}$$

$$\textbf{Higuchi model} \qquad ft = Q = K_H \times t^{1/2} \tag{5}$$

$$\textbf{Hixson Crowell model} \qquad W^{1/3} - W^{1/3} = kt \tag{6}$$

$$\textbf{Korsmeyer} - \textbf{Peppas model} \quad ln\frac{M_t}{M_o} = n\ lnt + lnk \tag{7}$$

$$\textbf{Baker} - \textbf{Lonsdale model} \quad F_t = \frac{2}{3}\left[1 - (1 - \frac{M_t}{M_o})^{\frac{2}{3}}\right]\frac{M_t}{M_o} = k(t)^{0.5} \tag{8}$$

Whereas $\mathbf{M_t}$ = The amount of drug released at time **t**, $\mathbf{K_o}$, **K** and $\mathbf{K_H}$ are constants.

3.7. Statistical analysis

The variance analysis for repeating values was calculated through ANOVA followed by Student's *t*-test (Turkey's post hoc test). The results were performed in triplicate with n = 3 and P-value < 0.05.

4. Results and discussions

4.1. Preface

We have designed a detailed project for the care and treatment of malignant melanoma skin cancer using in two steps. Step-I, we have synthesized nanodrugs (nanocarriers) by loading 5FU into rGO. It was then coated and stabilized. The successful synthesis of nanodrug was characterized by Transmission electron microscopy (TEM) to determine nano-structure, Atomic force microscope (AFM) surface roughness and topography, hydrodynamic particle and Zeta potential. Step-II, we have loaded and crosslinked (with different conc. of TEOS) nanodrug into modified arabinoxylan (CMARX) extracted from the natural resource (*Plantago Ovata*). The synthesized nanodrug was loaded into a polymeric matrix of CMARX at different TEOS concentrations to optimize the release of nanodrug from the polymeric matrix of nanocomposite hydrogels. We have conducted FTIR, SEM water contact angle, swelling and biodegradation analysis to determine structural, morphological, water contact angle (hydrophilicity/hydrophilicity), swelling and biodegradation behavior of these nanocomposite hydrogels. The release of 5FU was determined at different pH, anticancer activities were conducted and cell morphology was observed, the antibacterial activites were studied against severe disease causing pathogens, to optimize drug release the drug release kinetics were studied through different mathematical models to obtain best fitting model for anticancer activities.

The transmission electron spectroscopy (TEM) confirms the nano size of nanodrug, as mentioned in Fig. 1A & B. The nanodrug is present in the form of clusters. The nanodrug has a size of 320.59 ± 17.41 nm with − 32.1 ± 2.3 mV Zeta potential. The surface topography was observed using AFM images of the nano-drug in Fig. 1C & 1D. Three dimensions (3D) of the rGO-5FU as mentioned in Fig. 1C and two dimensional (2D) as shown in Fig. 1D, presents the rough surface topography due to rGO nanosheets (Rodzinski et al., 2016). The 5FU is loaded successfully on rGO, mixed perfectly, and the rough morphology is due to the presence of rGO-5FU sheets, as mentioned in Fig. 1C and 1D. The decrease in Zeta potential of the nano-drug is approximately 7.42 mV, as illustrated in Fig. 2E. The nanodrug size increases, and it is found to be 395.73 ± 37.47 nm after loading FU-5 in Fig. 1F. The controlled and sustained drug release was investigated at 6.8 pH at 37 °C to target the cancer cells (Zhu et al., 2009).

The nanodrug has been incorporated into carboxymethyl-arabinoxylan (CMARX) using different TEOS amounts as a crosslinker to get the best optimum nanocomposite hydrogel for care and treatment of malignant melanoma skin cancer. The drug release kinetics was studied, and *in-vitro* activity was performed against *U-87* cell lines to optimize the results.

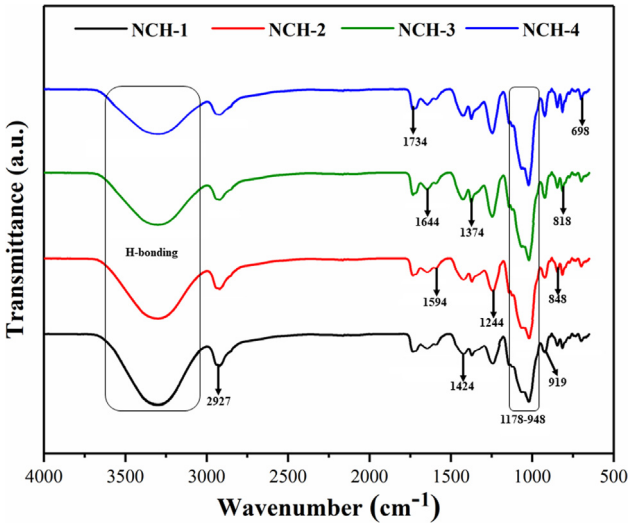

Fig. 2 Presents FTIR spectra of all composite hydrogels and different peaks are attributed to the composite hydrogels' different functionalities.

4.2. FTIR analysis

Fig. 2 presents the FTIR-spectrum of the nanocomposite hydrogels. The functional groups and the chemical interactions were identified via FTIR-spectrum by characteristic absorption peaks of the nanocomposite hydrogels (Zhao et al., 2018; Rodzinski et al., 2016; SreeHarsha et al., 2019). The increasing intensity of the absorption peak from 1110 to 1000 cm^{-1} was attributed to Si–O–C and Si–O–Si (asymmetric stretching), which confirms TEOS's crosslinking. The presence of an absorption peak at 1734 cm^{-1} corresponds to the hydrogen bonding of the natural polymers. The vibration peak 1644 cm^{-1} presents the C = C (stretching vibrations). The samples attributed characteristics absorption peaks of oxygen-based functional groups at 1595 cm^{-1}, 1424 cm^{-1}, and 1374 cm^{-1} for C = O (C = O stretching), C – O (C – O – C stretching) and C – O (C – OH, stretching) respectively (Zhang et al., 2010; Xu et al., 2015). The broadband at 3500–3100 cm^{-1} presents the characteristic absorption of O – H stretching. This absorption also describes intramolecular and intermolecular hydrogen bonding (Dash et al., 2010). The broad absorption peaks from 1178 to 948 and 919 cm^{-1} present the saccharine structure and pyranose ring. The absorption peak 2927 cm^{-1} indicates – CH_2 group (stretching mode) and confirms CMARX (Khan et al., 2020).

4.3. SEm

The surface morphology of the nanocomposite hydrogels was analyzed through SEM (Fig. 3). The surface morphology of all samples seemed smooth and uniform, and the red arrows indicate the nanodrug, which becomes more visible as the quantity of TEOS increases (Gao et al., 2019). The nanodrug alters the topography of the nanocomposite hydrogels. This rough morphology has a significant impact on cell adherence and sustained release of therapeutic agents to treat and care for skin cancer (Li et al., 2019). The hydrogels with rougher surfaces facilitate the exchange of gases and waste. Since the cancer cells increase more rapidly in a hypoxic environment; consequently, the exchange of gases and waste is essential for healthy cell proliferation and to kill the cancer cells. The rougher morphology of nanocomposite hydrogels significantly influences the normal cell adherence and proliferation. These nanocomposite hydrogels are more useful against *U-87* cell lines, which can be attributed to surface morphology variations (Nogueira and Hay, 2013; Zustiak et al., 2016). The red arrows exhibit the clusters of nanodrugs due to dried nanocomposite hydrogels. We can see the uniform distribution of nanodrug in NCH-1 due to less packing of hydrogel networking because of less crosslinking. Whereas NCH-4 exhibited maximum clustering of nanodrug due to closely packing because of the maximum crosslinking.

4.4. Wettability

We have observed nanocomposite hydrogels' wetting behavior is essential to interact with the body fluid in the clinical setting, such as on human skin. The wetting behavior of the materials is used to investigate the surface hydrophilicity and hydrophobicity. Typically, a lower water content angle (WCA) presents the hydrophilicity, and a higher contact angle signifies the hydrophobic nature of the materials. The polymeric matrix of nanocomposite hydrogel contains different functional groups (i.e., –OH, –COOH, –CH2, –NH2, etc.), and these functional groups aid up to a hydrophilic or hydrophobic behavior. The reducing degree of water contact angle is taken as a function against time—the increasing amount of crosslinking shifts the wetting trend from hydrophilic to hydrophobic. The decrease in water contact angle was found as time was increased, indicating a shift in the hydrophobic behavior to the hydrophilic side as in Fig. 4. Wetting behavior is necessary, as the wetting phenomenon improves material properties and surface action for biological activities (Huang et al., 2016). Since 5FU was loaded in rGO, the resulting rGO-5FU-CMARX nanocomposite hydrogels behave hydrophobically (Pourjavadi et al., 2020). Hydrophilic nature

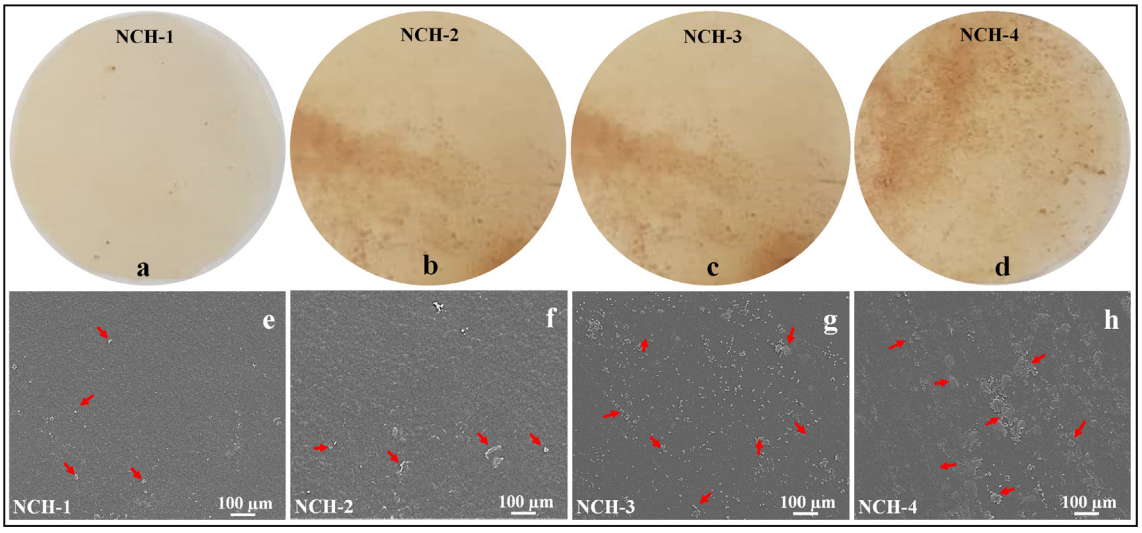

Fig. 3 Illustrates the micrographs (a, b, c and d) and surface morphology (e, f, g and) dried nanocomposite hydrogels containing nanodrug. The red arrows are presenting the nanodrug clusters during the drying process.

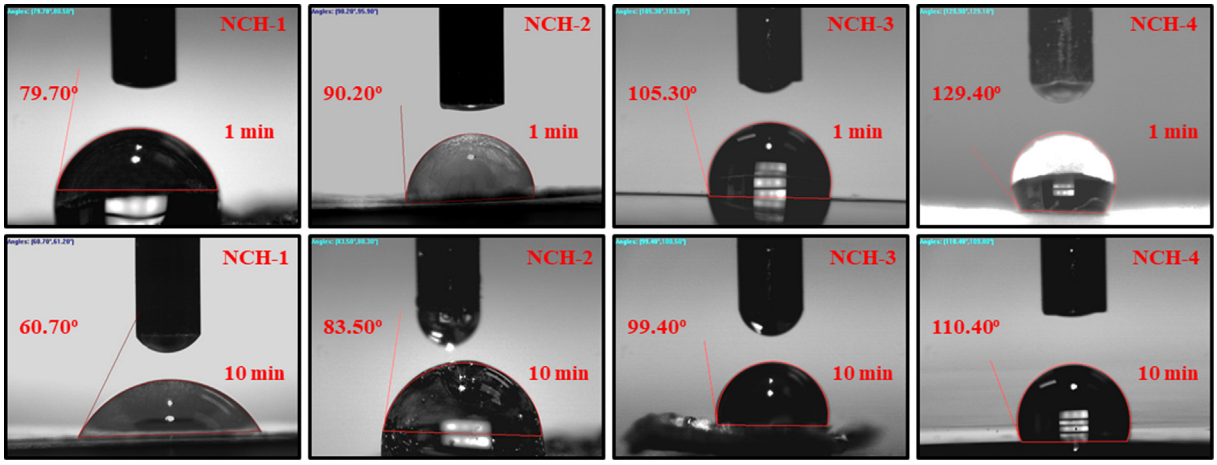

Fig. 4 Wetting nanocomposite hydrogel behavior at a different time interval (1 and 10 min) hydrophilicity and hydrophobicity of all composite hydrogels at zero second time.

increases the time taken to releases the nanodrug. With time, this hydrophobic trend shifts towards hydrophilic. We found an increase in hydrophobicity from NCH1 to NCH-4 due to an increase in the TEOS amount. The difference in water contact angle confirms the successful crosslinking of TEOS with CMARX. The NCH-4 was most hydrophobic among all nanocomposite hydrogels due to maximum amount of TEOS that engages –OH groups during crosslinking and nano-drug interaction (Liang et al., 2000). At the same time, NCH-1 was more hydrophilic due to freely available –OH groups at its surface, which facilitating hydrogen bonding (H-bonding). We suppose that hydroxyl groups cause to increase or decrease water contact angle due to H-bonding with water molecules (Tan et al., 2008).

4.5. Swelling

The nanocomposite hydrogel's swelling properties are vital for keeping the skin hydrated. These hydrogels absorb skin wound exudate and provide the required moisture to protect the soft tissues (Kamoun et al., 2017). Since malignant melanoma skin cancer pH is 6.8, we have observed the swelling analysis in water and PBS media having 6.8 pH at 37 °C as in Fig. 5A. All nanocomposite hydrogels' swelling behavior was maximum in aqueous media, and less swelling was found in PBS media. The nanocomposite hydrogel NCH-1 has exhibited less swelling, and NCH-4 has presented maximum swelling due to different amounts of crosslinkers. The nanocomposite hydrogel with less TEOS shows less crosslinking, and was unable to contain more water content, and presented little swelling (NCH-1). In comparison, NCH-4 presented more swelling due to maximum amount of TEOS that caused mature crosslinking and more water absorption capabilities. Increasing crosslinking in hydrogel beyond a specific limit decreases swelling property and starts losing water due to decreasing H-bonding. Losing water indicates that the wetting behavior of hydrogel is shifting from hydrophilic to hydrophobic (Du et al., 2017).

4.6. Biodegradation

An ideal hydrogel for skin cancer treatment is the one that releases the therapeutic agents on degradation (Hu et al., 2017). We have analyzed the nanocomposite hydrogels' biodegradation in PBS solution to mimic the human body conditions closely. The nanocomposite hydrogels' biodegradation was studied under standard *in-vitro* conditions to optimize our crosslinking for sustained and controlled nanodrug release. These nanocomposite hydrogels (NCH-1 to NCH-4) exhibited different biodegradation behavior due to weight loss (Fig. 5B. The presence of alkyl linkage and glycosidic bonds into MCARX also responded towards biodegradation. The disorientation of these glycosidic bonds contributed to the degradation of nanocomposite hydrogels (Hong et al., 2007). The increasing amount of TEOS caused more crosslinking and NCH-4 with the maximum amount of TEOS and exhibited little degradation due to the closely packed polymeric structure. The hydrogel sample NCH-1 presented more degradation due to less crosslinking as compare to NCH-4. The increasing amount of TEOS increases the hydrophobic behavior and secure packing due to more crosslinking. Hence, the biodegradation of the nanocomposite hydrogels can be controlled to optimize nanodrug release. The breakage of alkyl linkage and glycosidic bonds also leads to the biodegradation of the nanocomposite hydrogels (McBath and Shipp, 2010).

4.7. In vitro analysis

4.7.1. Antibacterial activities

The antibacterial activities of nanocomposite hydrogels were tested against pathogens *S. aureus* and *P. aeruginosa* as shown in Fig. 6A. These are well-known pathogens for causing severe skin diseases. The antibacterial activities were analyzed through zones inhibition against nanocomposite hydrogels NCH1-4. We hypothesize a synergistic antibacterial mechanism of nanocomposite hydrogels, as shown in Fig. 6A. The reduced GO nanosheets contain some multifunctional oxygen-containing structure and it with bacterial cell wall (Linklater et al., 2018). Howover, a large surface area of rGO may cause Wander-Waal's and π- π stacking interactions with the bacterial cell wall. The sharp edges of rGO may penetrate by repturing the bacterial cell membrane, leading to necrosis. 5FU has already established a well-known inhibitor of DNA replication that is up-taken by bacterial cells and cause antibacterial activities (Singh et al., 2015). It also can

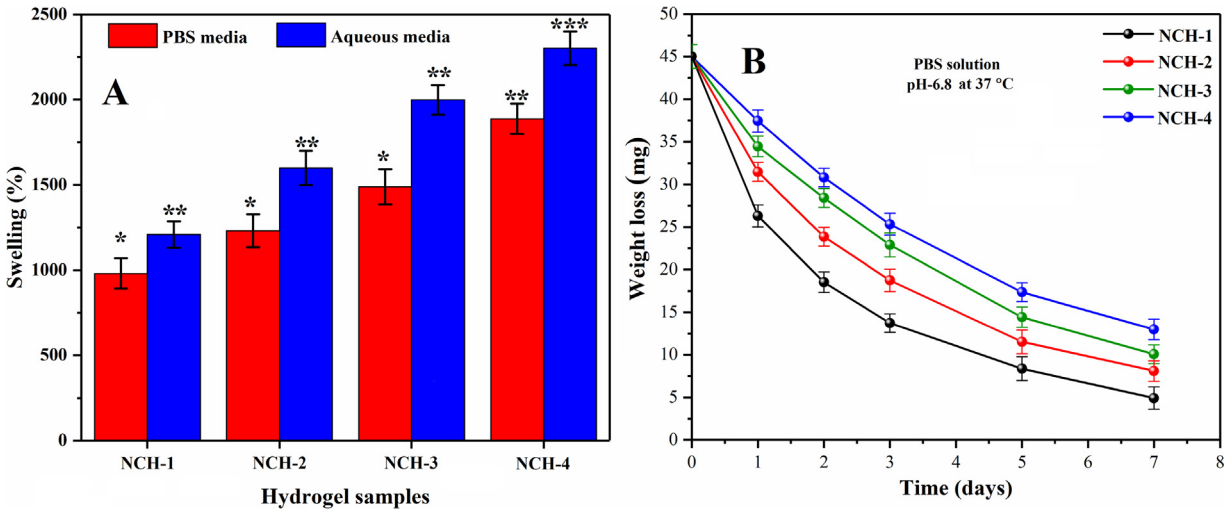

Fig. 5 (A) The swelling behavior of all composite hydrogel samples has shown different swelling behavior at different pH-media. (B) *In-vitro* biodegradation assay of all composite hydrogels samples has been studied in PBS solution (6.8-pH) at 37 ^{O}C. (*p < 0.05) and (n = 3).

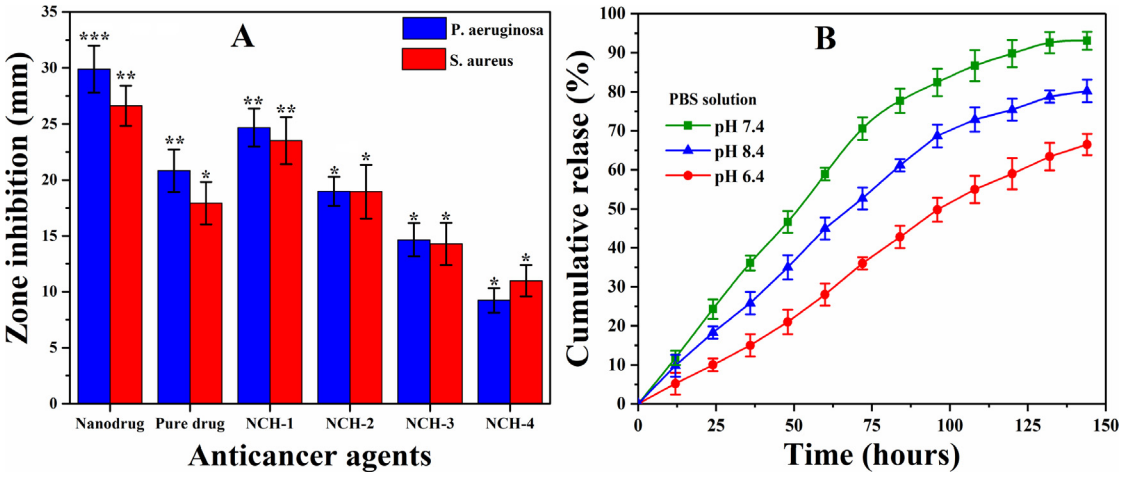

Fig. 6 (A) Presents the antibacterial activities of nanocomposite hydrogels and (B) *In vitro* transdermal drug release profile of skin cancer drug.

be explained as the hydrogels may have penetrated the bacterial wall and disrupted the protein synthesis by binding to bacterial ribosomes to hinder the bacterial activities and growth (Zykwinska et al., 2018).

The nanocomposite hydrogel NCH-1 was more antibacterial due to a quick release of nanodrug due to low crosslinking. The maximum inhibition zone was observed for NCH-1 compared to NCH-4 against *S. aureus* and *P. aeruginosa* as in Fig. 6A. It can be explained based on crosslinking as NCH-1 less amount of crosslinker that causes the quick release of nanodrug and NCH-4 maximum crosslink. That has a slow release of nanodrug as 5FU is also a well-known anticancer drug, which also causes antibacterial activities. All these factors may contribute to the hydrogel, rGO and 5FU towards antibacterial activities, which causes death or bacterial growth inhibition (Rangel-Vega et al., 2015). Hence, our nanocomposite hydrogel systems are attractive for the care and treatment of malignant melanoma skin cancer by preventing antibacterial infections.

4.7.2. In-vitro drug release

Since the last century, the transdermal delivery mechanism for drug administration has been generally utilized to treat disease conditions. The drugs are delivered to the target site through various skin layers into the bloodstreams with little or no systemic circulation. Franz diffusion has a preferable advantage over the conventional techniques due to avoiding the chemical and hostile environment of gastrointestinal. It can be used to consider other physiological contraindications while dealing with drugs with a short biological half-life. Fig. 6B shows the nanodrug permeation profile via the cellulose nitrate membrane. The results demonstrate considerable permeation and sustained nanodrug release under different pH media. It was obsereved that maxium drug release (93.10 %) was found in neutral media (pH = 7.4), minimum drug release (80.20 %) was found in acidic media (pH = 6.4), whereas, intermediate drug release (66.50 %) was obsereved in basic media (pH = 8.4). The dissolution of the drug and the enhancement

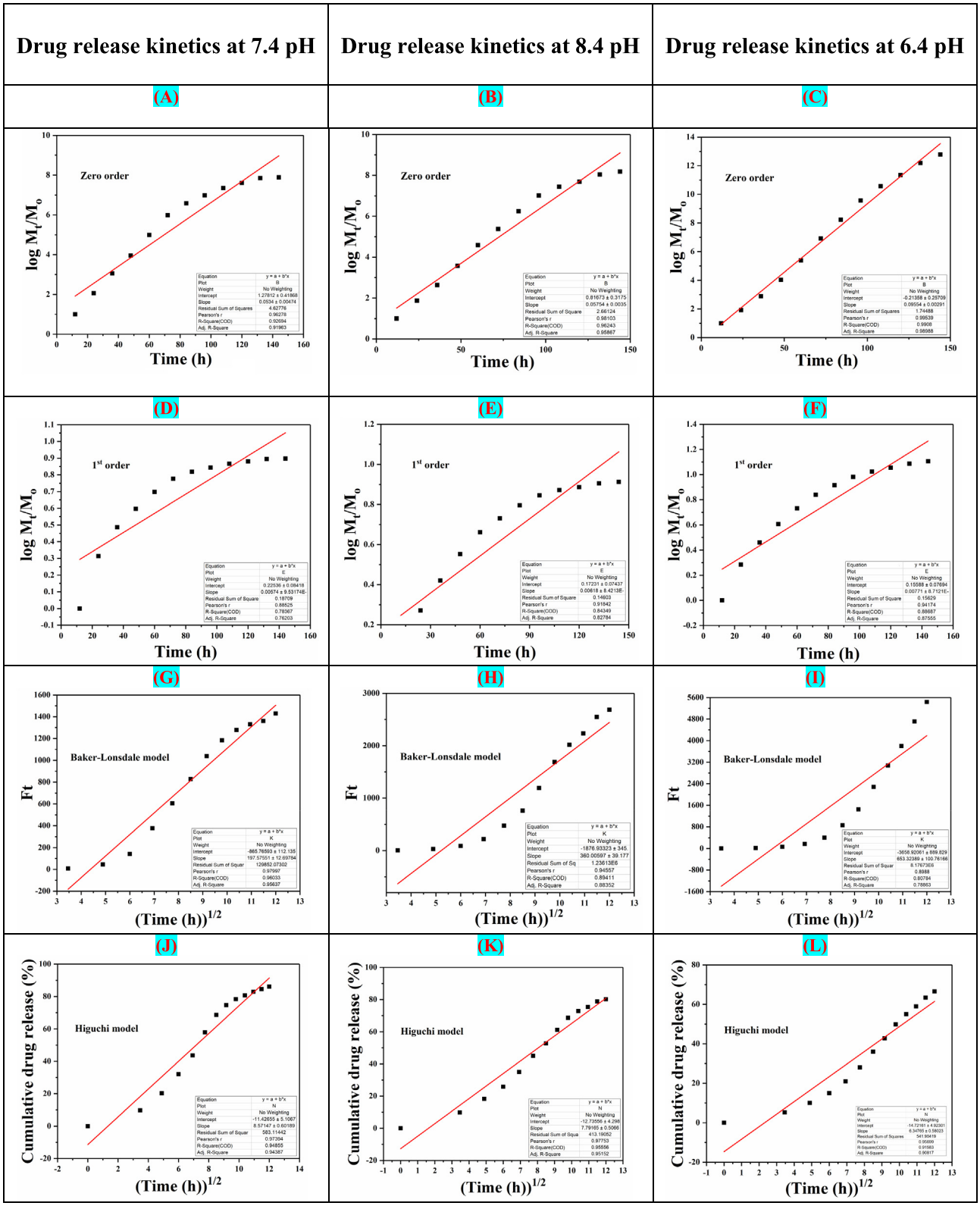

Fig. 7 The drug release kinetics models of NCH2 at different pH (6.4, 7.4 and 8.4): (A, B, C) Zero-order, (D, E, F) First-order, (G, H, I) Hixson Model, (J, K, L) Higuchi model, (M, N, O) Korsmeyer–Peppas model, (P, Q, R) Baker-Lonsdale model.

effects of the medium were attributed to nanodrug penetration through the epidermal diffusional barrier. Drug release is an essential process focused on controlled swelling and biodegradation of polymeric matrix (Abba et al., 2019). PBS has been used as a media that mimicked human body fluids. It contacts the medium between the cellulose nitrate membrane

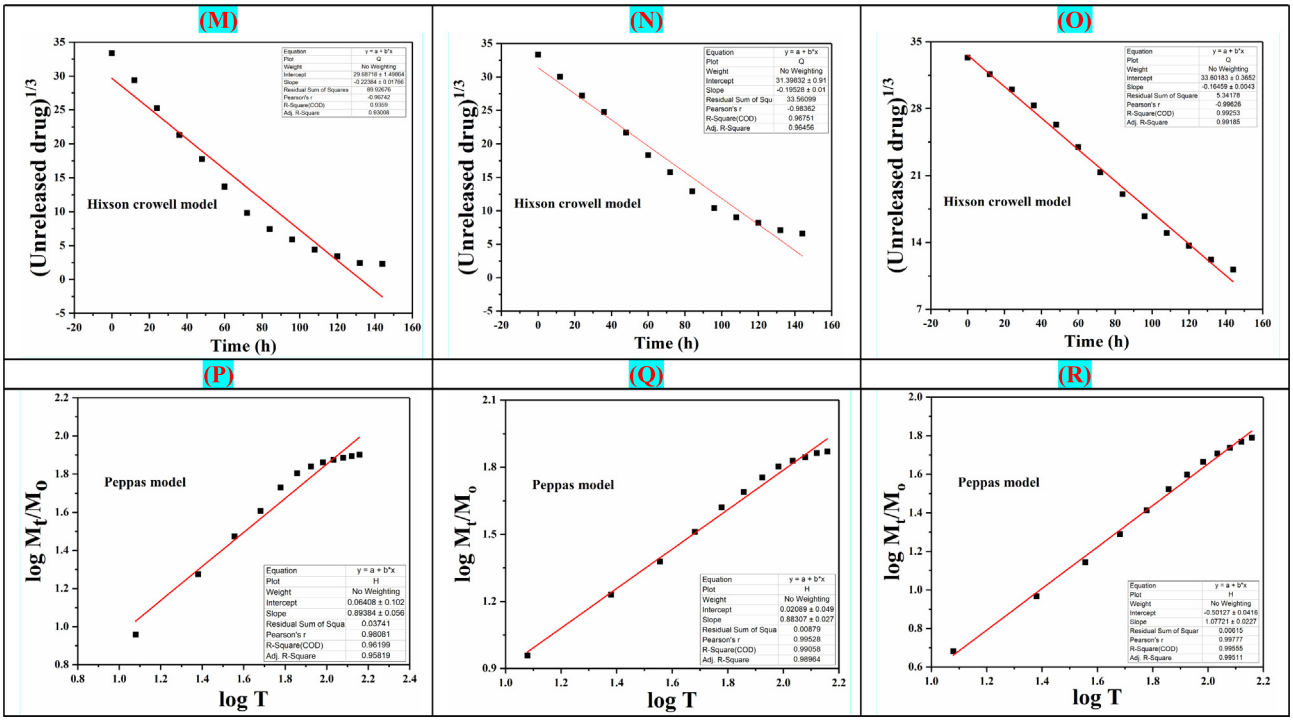

Fig. 7 (*continued*)

and the nanocomposite hydrogel membrane to facilitate the release of nanodrug (Sa'adon, 2019). Hence, these nanocomposite hydrogels may assist for targeted and sustained release of anticancer therapeutic, which helps care and treatment of malignant melanoma skin cancer.

4.7.3. Kinetics release of Fluorouracil

The mathematical models (Eqs. (4)–(9)) have been applied to determine the in-vitro drug (5FU) release kinetics as shown in Fig. 7. The chitosan matrix helps for controlled and sustained release from the nanocarrier. The swelling and erosion processes also affect the 5-FU release kinetics. The kinetic release of 5FU under different fitting models (i.e., zero and first order, Hixson–Crowell, Higuchi models, Korsmeyer–Peppas and Baker-Lonsdale) was studied. We have demonstrated the kinetic release behavior of 5FU. The regression coefficient (R^2) was presented (Table 1), and Korsmeyer-Peppas was the best-fitting model for the release of drugs at pH 8.4. At 6.4 pH. Korsmeyer-Peppas model, also known as "Power-law," was the best fitting model that describes the release of drugs from the polymeric system. The Power law describes the drug release mechanism under water diffusion, swelling, and dissolution of the polymeric matrix (Singhvi and Singh, 2011). Whereas, Baker-Lonsdale model was the best fitting model for release of drug at 7.4 pH that explains drug release from spherical matrices. Hence, from mathematical modeling, it was found that drug release adopted different modes at different pH.

4.7.4. Anticancer/Cytotoxic activity

The anticancer activities of the nanocomposite hydrogels have been demonstrated in Fig. 8. Apoptosis is a highly controlled mechanism of cell death without damaging the healthy tissue. It regulates the microenvironment, growth factors, deficiency of nutrients, metallic and polymeric nanoparticles to the targeted site. Mitochondria play a central role in the induced cytotoxicity of nanoparticles (Zhuang et al., 2018). The apoptotic initiation due to the release of 5FU from the nanocarrier has been reported previously, and rGO is well-known due to more surface-area and drug-loading capabilities (Ali et al., 2018).

This effectiveness can be attributed to the dual efficiency of our nanocomposite hydrogel system, and developed nanodrug contains Fluorouracil loaded onto rGO sheets. The rGO has already been reported for anticancer activity (Kavinkumar et al., 2017). The rGO and Fluorouracil, therefore, synergistically display their role for the anticancer activity of nanodrug. The hydrogel samples displayed activities, which in principally inversely related to the degree of crosslinking in the resulting hydrogel system. NCH1 has the lowest crosslinking and therefore displayed an increased anticancer activities aginst *U-87*. Nanodrug contained hydrogel samples NCH1-NCH4 displayed appreciable toxicity against *U-87* cell lines. The fabrication of nanocomposite hydrogels displayed appreciable anticancer activity against the *U-87* cell lines. Nanocomposite hydrogels displayed an enhanced efficiency compared to the pure 5FU, merely due to rapid drug release and delivery at the cancer microenvironment. On the contrary, NCH-4 is with the maximum crosslinking and exhibited delayed in biodegradation and drug-release, subsequently decreased anticancer potency.

This study was focused on the apoptotic response of our nanocomposite hydrogels against *U-87* cell lines. We analyzed the cell viability of *U-87* cell lines after treating them with nanocomposite hydrogels at a conc. 100 mg/mL for different time intervals (24, 48 & 72 h). The nanocomposite hydrogels'

Table 1 Summarises the drug release kinetics outcomes against various mathematical models to determine the best-fit model for drug release in terms of Interaction coefficient at different pH (6.4, 7.4 and 8.4).

	Models	Intercept	Regression coefficient (R^2)
Drug release kinetics at 7.4 pH	Zero-order	1.27812 ± 0.41868	0.92694
	First Order	0.22536 ± 0.0818	0.78367
	Baker-Lonsdale model	−865.76539 ± 112.135	0.97997
	Higuchi model	−11.57147 ± 5.1067	0.97394
	Hixon Crowell model	29.68718 ± 1.49864	0.9359
	Peppas model	0.06408 ± 0.102	0.96199
Drug release kinetics at 8.4 pH	Zero-order	1.27812 ± 0.41868	0.96248
	First Order	0.22536 ± 0.0818	0.84359
	Baker-Lonsdale model	−865.76539 ± 112.135	0.89411
	Higuchi model	−11.57147 ± 5.1067	0.95556
	Hixon Crowell model	29.68718 ± 1.49864	0.96751
	Peppas model	0.06408 ± 0.102	0.99058
Drug release kinetics at 6.4 pH	Zero-order	−0.21358 ± 0.25709	0.9908
	First Order	0.15588 ± 0.07694	0.88687
	Baker-Lonsdale model	−3658.92061 ± 889.829	0.80784
	Higuchi model	−14.72161 ± 4.92301	0.91583
	Hixon Crowell model	33.60183 ± 0.3652	0.99253
	Peppas model	−0.50127 ± 0.0416	0.99555

hydrophilicity has enhanced anticancer activities due to rappid interaction with the extracellular matrix (ECM). Increasing hydrophobicity caused poor adherence that does not let the proliferation of cancer cells. However, these composite hydrogels presented different degradation behavior in-vitro, as shown in Fig. 5B. The degradation of nanocomposite hydrogels also released nanodrug that actively participated in anticancer activity. Fig. 9 shows that NCH-1 was more active than NCH-4 against the *U-87* cell lines. It was observed as the low crosslinking of NCH-1 initiated a rapid biodegradation that released more nanodrug that caused maximum anticancer activity. NCH-1 was more active than other nanocomposite hydrogels against *U-87* cell lines due to the quick release of nanodrug because of low crosslinking.

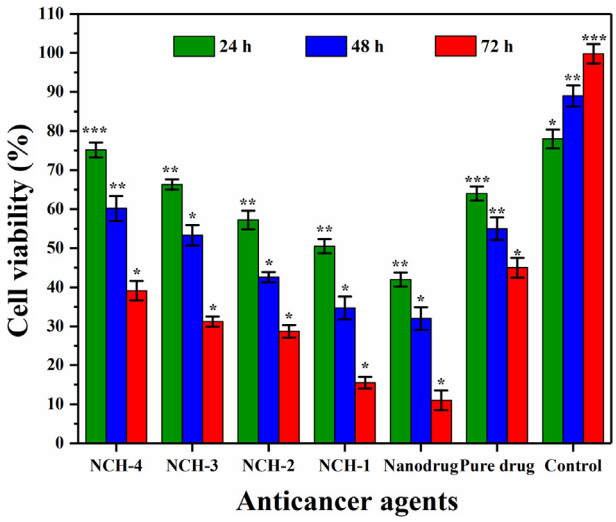

Fig. 8 Bar graph showing the percentage of cell viability against different anticancer agents. The cell viability was reduced as crosslinking increased from NCH-1 to NCH-4. Significance levels are indicated according to the legend *p < 0.05, **p < 0.01 and ***p < 0.001 and n = 3.

4.7.5. Cellular morphology against nanocomposite hydrogels

The nanocomposite hydrogels contact human tissue for several hours, and this close contact may cause cellular and tissue morphological changes. Henceforth, *U-87* cells were seeded over the well plate and hydrogels were poured over the culture cells and subsequently photographed at 24, 48 & 72 h of incubation. In comparison to +ive control cells. Fig. 9 shows that cell morphology of *U-87* cell lines when exposed to pure drugs, nanodrugs, and nanocomposite hydrogels. Initially, pure drug, nanodrug, and nanocomposite hydrogels supported cell adherence and growth with proper spreading shape after 24 h. After 24 h, a change in cell morphology was obsereved due to interaction of these anticancer therapeutic agents with *U-87* cell lines. The red circules are exhibiting cell clustering, red arrows are presenting dead cells and yellow arrows are indicating reuture cellular morphology. The cell clustering may be explained due to different distribution of rGO that have **π-π** stacking with high surface charge that may cause clustering of the *U-87*. It was observed that NCH-1 exhibited maximum anticancer activity than NCH-4 due to the quick releasing of nanodrug that caused maximum anticancer activities. It may be due to low crosslinking of TEOS, which response to a quick release of nanodrug that causes more anticancer activities against *U-87* cell lines. The nanocomposite hydrogels NCH-3 and NCH-4 were found to be less cytotoxic. However, NCH-2 and NCH-1 were found to have maximum anticancer activity due to the quick release of nanodrug system. It was also observed that pure drug caused less anticancer activities than nanodrug. The nanocomposite hydrogels have different cellular morphology with uniform anticancer activities.

5. Conclusions

We have reported the synthesis of nanodrug and loaded it into polymeric matrix of functionalized arabinoxylan (CMARX), which is extracted from *Plantago Ovata* with different

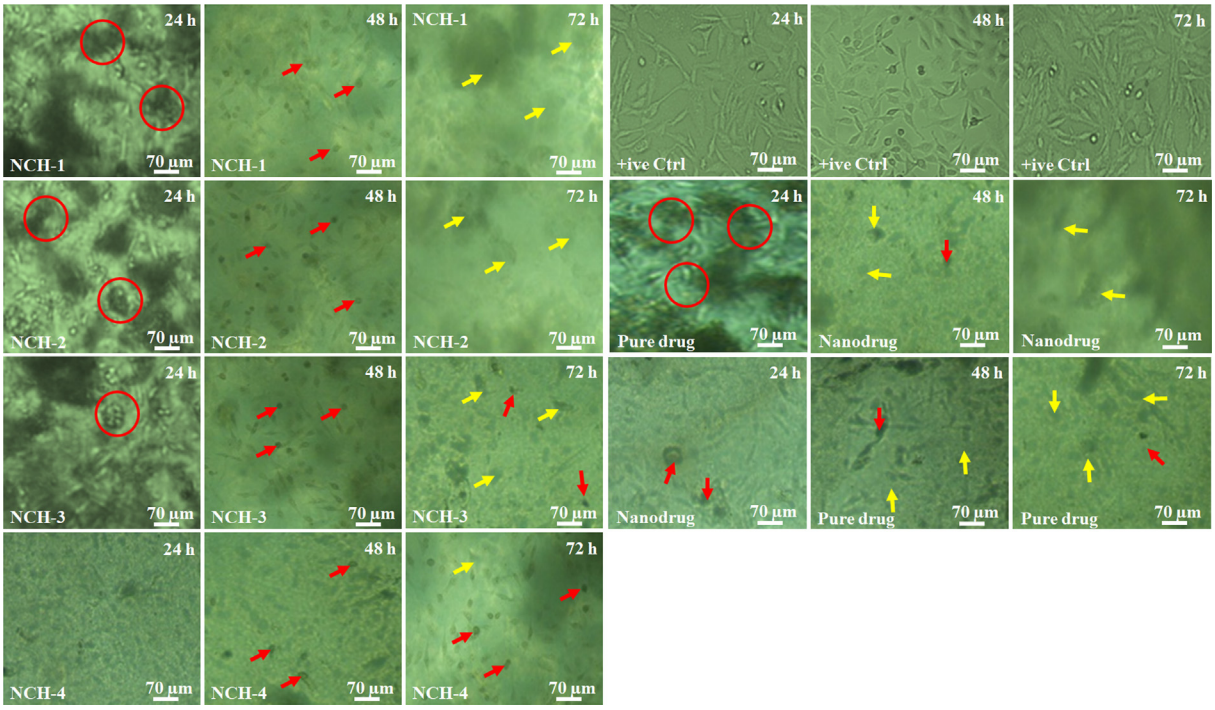

Fig. 9 Cell morphology against different anticancer agents at a different time interval (24, 48 and 72 h). The red circles show the cell cluster, red arrows indicating dead cells and yellow arrows present the rupture cell membrane.

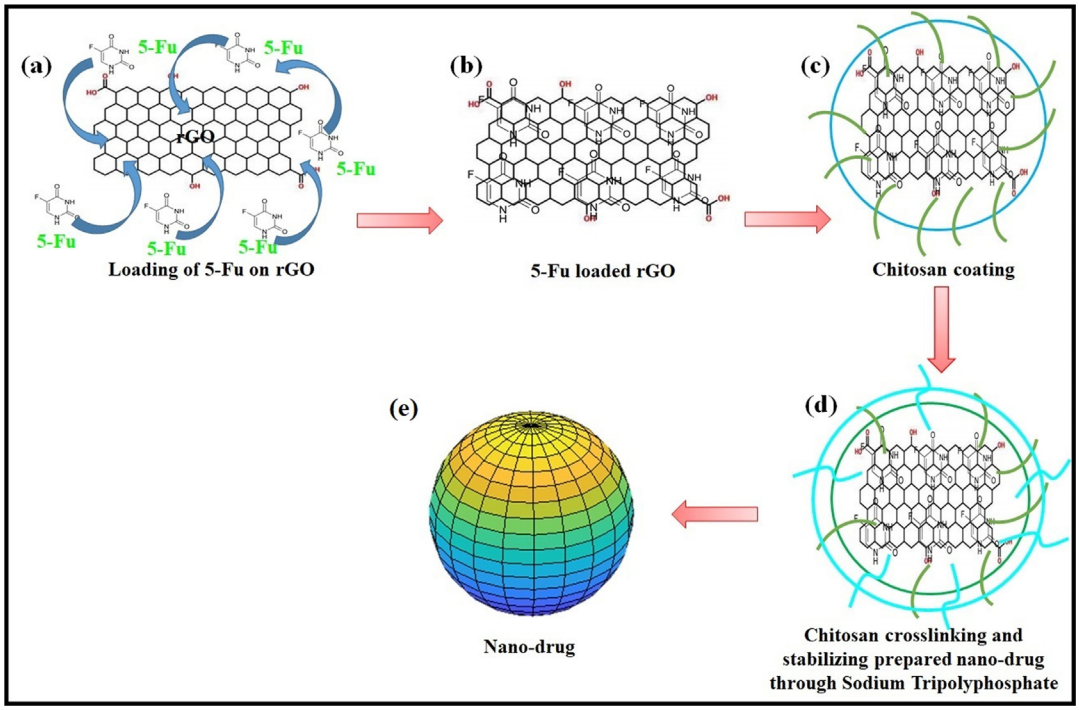

Scheme 1 Presents the synthesis of the nano-drug, (a) solution of 5FU and rGO, (b) loading of 5FU onto the rGO through a simply incubating for 24 h, (c) coating of chitosan (0.1%, w/v) using solvent gelation method, (d) crosslinking and stabilizing synthesized nanocomposite sodium tripolyphosphate (0.125%, w/v) and, (e) Nanodrug was got after centrifuging (15,000 for 30 min) drug nanocomposite and treated with lactose monohydrate (2%, w/v) as cryo-protectant.

formulations. After loading nanodrug into CMARX, it is crosslinked with different amounts of crosslinker (TEOS) to investigate various physicochemical factors and *in-vitro* activities, i.e., drug delivery via Franz diffusion method, antibacterial and anticancer activities were studied for the nanocomposite hydrogels. The FTIR spectral profile exhibits

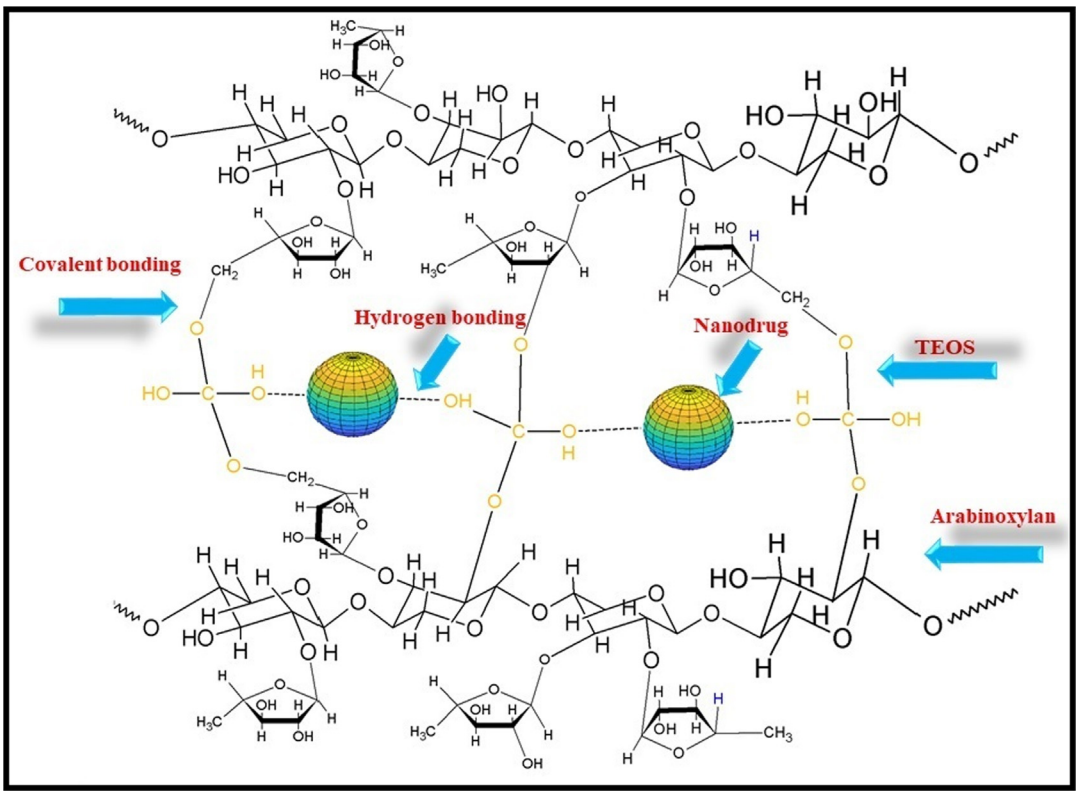

Scheme 2 Loading of nanodrug system and crosslinking CMARX with different amounts of TEOS as crosslinker via simple blending method. It also proposed that the nanodrug interacted through hydrogen bonding.

the successful crosslinking and presence of rGO based moieties. SEM analysis also presented the surface morphology of well-dried nanocomposite hydrogels. It exhibits a different amount of nanodrug over the surface due to different amounts of crosslinker. These nanocomposite hydrogels have exhibited different wetting responses. That leads to different swelling and biodegradation behavior, which plays a vital role in the sustained release of 5FU. The optimized swelling, biodegradation, and wetting properties help for sustain the release of therapeutic agents against bacterial and cancer activities for care and treatment of malignant melanoma skin cancer. These nanocomposite hydrogels have proven to be pH-sensitive under different pH conditions for sustained and controlled release of 5FU. Moreover, NCH-1 presents significantly high antibacterial and anticancer activities against *S. aureus* and *P. aeruginosa and U-87* cell lines, respectively. It may be due to the excess release of nanodrug from hydrogel on biodegradation because of little crosslinking compared to other composite hydrogel samples (NCH-2, NCH-3 and NCH-4). The results exhibited that NCH1-4 could be useful in the care and treatment of malignant melanoma skin cancer. Hence, we propose that nanocomposite hydrogels NCH1-4 can serve as a guideline to develop future biomaterials for skin cancer treatment.

CRediT authorship contribution statement

Samina Nazir: Formal analysis, Funding acquisition, Methodology. **Muhammad Umar Aslam Khan:** Conceptualization, Data curation, Formal analysis, Funding acquisition, Investigation, Methodology, Software, Supervision, Validation, Visualization, Writing - original draft, Writing - review & editing. **Wafa Shamsan Al-Arjan:** Data curation, Formal analysis, Methodology, Writing - review & editing. **Saiful Izwan Abd Razak:** Conceptualization, Funding acquisition, Investigation, Project administration, Resources, Writing - review & editing. **Aneela Javed:** Formal Analysis, Resources, Validation. **Mohammed Rafiq Abdul Kadir:** Funding acquisition, Investigation, Project administration, Resources, Supervision.

Declaration of Competing Interest

The authors declare that they have no known competing financial interests or personal relationships that could have appeared to influence the work reported in this paper.

Acknowledgment

The authors extend their appreciation to the Deputyship for Research & Innovation, Ministry of Education in Saudi Arabia, for funding this research work through the project number IFT20142, under Institutional Financing Track 2020, King Faisal University.

Authors Contribution

Conceptualization, Muhammad Umar Aslam Khan, Saiful Izwan Abd Razak; **Data curation**, Muhammad Umar Aslam Khan and Wafa Shamsan Al-Arjan; **Formal analysis**,

Muhammad Umar Aslam Khan, Samina Nazir, and Wafa Shamsan Al-Arjan; **Funding acquisition**, Muhammad Umar Aslam Khan, Samina Nazir, Saiful Izwan Abd Razak and Mohammed Rafiq Abdul Kadir; **Investigation**, Muhammad Umar Aslam Khan, Saiful Izwan Abd Razak and Mohammed Rafiq Abdul Kadir; **Methodology**, Muhammad Umar Aslam Khan, Samina Nazir and Wafa Shamsan Al-Arjan; **Project administration**, Saiful Izwan Abd Razak and Mohammed Rafiq Abdul Kadir; **Resources**, Mohammed Rafiq Abdul Kadir, Saiful Izwan Abd Razak and Aneela Javeed; **Software**, Muhammad Umar Aslam Khan; **Supervision**, Saiful Izwan Abd Razak and Mohammed Rafiq Abdul Kadir; **Validation**: Muhammad Umar Aslam Khan and Aneela Javeed; **Visualization**, Muhammad Umar Aslam Khan,; **Writing–original draft**, Muhammad Umar Aslam Khan; **Writing – review & editing**, Muhammad Umar Aslam Khan and Saiful Izwan Abd Razak. Wafa Shamsan Al-Arjan helped in the revision of the manuscript.

References

Abba, M., Ibrahim, Z., Chong, C.S., Zawawi, N.A., Kadir, M.R.A., Yusof, A.H.M., Abd Razak, S.I., 2019. Transdermal delivery of crocin using bacterial nanocellulose membrane. Fibers Polym. 20 (10), 2025–2031.

Ali, D., Alarifi, S., Alkahtani, S., Almeer, R.S., 2018. Silver-doped graphene oxide nanocomposite triggers cytotoxicity and apoptosis in human hepatic normal and carcinoma cells. Int. J. Nanomed. 13, 5685.

Alkafajy, A.M., Albayati, T.M., 2020. High performance of magnetic mesoporous modification for loading and release of meloxicam in drug delivery implementation. Mater. Today Commun. 23, 100890.

Dash, S., Murthy, P.N., Nath, L., Chowdhury, P., 2010. Kinetic modeling on drug release from controlled drug delivery systems. Acta Pol. Pharm. 67 (3), 217–223.

Deb, A., Vimala, R., 2018. Natural and synthetic polymer for graphene oxide mediated anticancer drug delivery—a comparative study. Int. J. Biol. Macromol. 107, 2320–2333.

Dong, P., Rakesh, K., Manukumar, H., Mohammed, Y.H.E., Karthik, C., Sumathi, S., Mallu, P., Qin, H.-L., 2019. Innovative nano-carriers in anticancer drug delivery-a comprehensive review. Bioorg. Chem. 85, 325–336.

Du, X., Wang, J., Cui, H., Zhao, Q., Chen, H., He, L., Wang, Y., 2017. Breath-taking patterns: discontinuous hydrophilic regions for photonic crystal beads assembly and patterns revisualization. ACS Appl. Mater. Interfaces 9 (43), 38117–38124.

Gao, Y., Ding, S., Huang, X., Fan, Z., Sun, J., Hai, Y., Li, K., 2019. Development and evaluation of hollow mesoporous silica microspheres bearing on enhanced oral delivery of curcumin. Drug Dev. Ind. Pharm. 45 (2), 273–281.

Gordon, R., 2013. In Skin cancer: an overview of epidemiology and risk factors, Seminars in oncology nursing, 2013; Elsevier: pp 160-169.

Hong, Y., Song, H., Gong, Y., Mao, Z., Gao, C., Shen, J., 2007. Covalently crosslinked chitosan hydrogel: properties of in vitro degradation and chondrocyte encapsulation. Acta Biomater. 3 (1), 23–31.

Hu, J., Chen, Y., Li, Y., Zhou, Z., Cheng, Y., 2017. A thermodegradable hydrogel with light-tunable degradation and drug release. Biomaterials 112, 133–140.

Huang, Y., Hao, M., Nian, X., Qiao, H., Zhang, X., Zhang, X., Song, G., Guo, J., Pang, X., Zhang, H., 2016. Strontium and copper co-substituted hydroxyapatite-based coatings with improved antibacterial activity and cytocompatibility fabricated by electrodeposition. Ceram. Int. 42 (10), 11876–11888.

Huang, T.-D., Poirel, L., Bogaerts, P., Berhin, C., Nordmann, P., Glupczynski, Y., 2014. Temocillin and piperacillin/tazobactam resistance by disc diffusion as antimicrobial surrogate markers for the detection of carbapenemase-producing Enterobacteriaceae in geographical areas with a high prevalence of OXA-48 producers. J. Antimicrob. Chemother. 69 (2), 445–450.

Jahromi, L.P., Ghazali, M., Ashrafi, H., Azadi, A., 2020. A comparison of models for the analysis of the kinetics of drug release from PLGA-based nanoparticles. Heliyon 6, (2) e03451.

Kamoun, E.A., Kenawy, E.-R.S., Chen, X., 2017. A review on polymeric hydrogel membranes for wound dressing applications: PVA-based hydrogel dressings. J. Adv. Res. 8 (3), 217–233.

Karimi, M., Eslami, M., Sahandi-Zangabad, P., Mirab, F., Farajisafiloo, N., Shafaei, Z., Ghosh, D., Bozorgomid, M., Dashkhaneh, F., Hamblin, M.R., 2016. pH-Sensitive stimulus-responsive nanocarriers for targeted delivery of therapeutic agents. Wiley Interdiscip. Rev. Nanomed. Nanobiotechnol. 8 (5), 696–716.

Kavinkumar, T., Varunkumar, K., Ravikumar, V., Manivannan, S., 2017. Anticancer activity of graphene oxide-reduced graphene oxide-silver nanoparticle composites. J. Colloid Interface Sci. 505, 1125–1133.

Khan, M.U.A., Al-Thebaiti, M.A., Hashmi, M.U., Aftab, S., Abd Razak, S.I., Abu Hassan, S., Abdul Kadir, M.R., Amin, R., 2020. Synthesis of Silver-Coated Bioactive Nanocomposite Scaffolds Based on Grafted Beta-Glucan/Hydroxyapatite via Freeze-Drying Method: Anti-Microbial and Biocompatibility Evaluation for Bone Tissue Engineering. Materials 13 (4), 971.

Khan, M.I., An, X., Dai, L., Li, H., Khan, A., Ni, Y., 2019. Chitosan-based polymer matrix for pharmaceutical excipients and drug delivery. Curr. Med. Chem. 26 (14), 2502–2513.

Khan, M.U.A., Raza, M.A., Razak, S.I.A., Abdul Kadir, M.R., Haider, A., Shah, S.A., Mohd Yusof, A.H., Haider, S., Shakir, I., Aftab, S., 2020. Novel functional antimicrobial and biocompatible arabinoxylan/guar gum hydrogel for skin wound dressing applications. J. Tissue Eng. Regener. Med.

Li, Q., Wen, J., Liu, C., Jia, Y., Wu, Y., Shan, Y., Qian, Z., Liao, J., 2019. Graphene-nanoparticle-based self-healing hydrogel in preventing postoperative recurrence of breast cancer. ACS Biomater. Sci. Eng. 5 (2), 768–779.

Liang, L., Rieke, P.C., Liu, J., Fryxell, G.E., Young, J.S., Engelhard, M.H., Alford, K.L., 2000. Surfaces with reversible hydrophilic/hydrophobic characteristics on crosslinked poly (N-isopropylacrylamide) hydrogels. Langmuir 16 (21), 8016–8023.

Linklater, D.P., Baulin, V.A., Juodkazis, S., Ivanova, E.P., 2018. Mechano-bactericidal mechanism of graphene nanomaterials. Interface focus 8 (3), 20170060.

McBath, R.A., Shipp, D.A., 2010. Swelling and degradation of hydrogels synthesized with degradable poly (β-amino ester) crosslinkers. Polym. Chem. 1 (6), 860–865.

Misra, R., Sahoo, S.K., 2010. Intracellular trafficking of nuclear localization signal conjugated nanoparticles for cancer therapy. Eur. J. Pharm. Sci. 39 (1–3), 152–163.

Moscovici, M., 2015. Present and future medical applications of microbial exopolysaccharides. Front. Microbiol. 6, 1012.

Nogueira, V., Hay, N., 2013. Molecular pathways: reactive oxygen species homeostasis in cancer cells and implications for cancer therapy. Clin. Cancer Res. 19 (16), 4309–4314.

Pourjavadi, A., Asgari, S., Hosseini, S.H., 2020. Graphene oxide functionalized with oxygen-rich polymers as a pH-sensitive carrier for co-delivery of hydrophobic and hydrophilic drugs. J. Drug Delivery Sci. Technol. 56, 101542.

Rangel-Vega, A., Bernstein, L.R., Mandujano Tinoco, E.-A., García-Contreras, S.-J., García-Contreras, R., 2015. Drug repurposing as an alternative for the treatment of recalcitrant bacterial infections. Front. Microbiol. 6, 282.

Rodzinski, A., Guduru, R., Liang, P., Hadjikhani, A., Stewart, T., Stimphil, E., Runowicz, C., Cote, R., Altman, N., Datar, R., 2016.

Targeted and controlled anticancer drug delivery and release with magnetoelectric nanoparticles. Sci. Rep. 6 (1), 1–14.

Sa'adon, S., Razak, S.I.A., Fakhruddin, K., 2019. Drug-loaded polyvinyl alcohol electrospun nanofibers for transdermal drug delivery: review on factors affecting the drug release. Proc. Comput. Sci., 2019, 158, 436-442.

Saghir, S., Iqbal, M.S., Hussain, M.A., Koschella, A., Heinze, T., 2008. Structure characterization and carboxymethylation of arabinoxylan isolated from Ispaghula (Plantago ovata) seed husk. Carbohydr. Polym. 74 (2), 309–317.

Schaible, U.E., Stefan, H., 2007. Malnutrition and infection: complex mechanisms and global impacts. PLoS med 4, (5) e115.

Shah, S.A., Khan, M.A., Arshad, M., Awan, S., Hashmi, M., Ahmad, N., 2016. Doxorubicin-loaded photosensitive magnetic liposomes for multi-modal cancer therapy. Colloids Surf., B 148, 157–164.

Singh, V., Brecik, M., Mukherjee, R., Evans, J.C., Svetlíková, Z., Blaško, J., Surade, S., Blackburn, J., Warner, D.F., Mikušová, K., 2015. The complex mechanism of antimycobacterial action of 5-fluorouracil. Chem. Biol. 22 (1), 63–75.

Singhvi, G., Singh, M., 2011. In-vitro drug release characterization models. Int. J. Pharm. Stud. Res. 2 (1), 77–84.

SreeHarsha, N., Maheshwari, R., Al-Dhubiab, B.E., Tekade, M., Sharma, M.C., Venugopala, K.N., Tekade, R.K., Alzahrani, A.M., 2019. Graphene-based hybrid nanoparticle of doxorubicin for cancer chemotherapy. Int. J. Nanomed. 14, 7419.

Tan, G., Wang, Y., Li, J., Zhang, S., 2008. Synthesis and characterization of injectable photocrosslinking poly (ethylene glycol) diacrylate based hydrogels. Polym. Bull. 61 (1), 91–98.

Thakur, R., Florek, C., Kohn, J., Michniak, B., 2008. Electrospun nanofibrous polymeric scaffold with targeted drug release profiles for potential application as wound dressing. Int. J. Pharm. 364 (1), 87–93.

Thambi, T., Li, Y., Lee, D.S., 2017. Injectable hydrogels for sustained release of therapeutic agents. J. Control. Release 267, 57–66.

Trovatti, E., Freire, C.S., Pinto, P.C., Almeida, I.F., Costa, P., Silvestre, A.J., Neto, C.P., Rosado, C., 2012. Bacterial cellulose membranes applied in topical and transdermal delivery of lidocaine hydrochloride and ibuprofen: in vitro diffusion studies. Int. J. Pharm. 435 (1), 83–87.

Uddin, M.J., Scoutaris, N., Klepetsanis, P., Chowdhry, B., Prausnitz, M. R., Douroumis, D., 2015. Inkjet printing of transdermal microneedles for the delivery of anticancer agents. Int. J. Pharm. 494 (2), 593–602.

Uddin, M.J., Scoutaris, N., Economidou, S.N., Giraud, C., Chowdhry, B.Z., Donnelly, R.F., Douroumis, D., 2020. 3D printed microneedles for anticancer therapy of skin tumours. Mater. Sci. Eng., C 107, 110248.

Valgas, C., Souza, S.M.d., Smânia, E.F., Smânia Jr, A., 2007. Screening methods to determine antibacterial activity of natural products. Brazil. J. Microbiol., 2007, 38, (2), 369-380.

Xu, C., Shi, X., Ji, A., Shi, L., Zhou, C., Cui, Y., 2015. Fabrication and characteristics of reduced graphene oxide produced with different green reductants. PLoS ONE 10, (12) e0144842.

Zhang, J., Yang, H., Shen, G., Cheng, P., Zhang, J., Guo, S., 2010. Reduction of graphene oxide via L-ascorbic acid. Chem. Commun. 46 (7), 1112–1114.

Zhao, X., Wei, Z., Zhao, Z., Miao, Y., Qiu, Y., Yang, W., Jia, X., Liu, Z., Hou, H., 2018. Design and development of graphene oxide nanoparticle/chitosan hybrids showing pH-sensitive surface charge-reversible ability for efficient intracellular doxorubicin delivery. ACS Appl. Mater. Interfaces 10 (7), 6608–6617.

Zhu, L., Ma, J., Jia, N., Zhao, Y., Shen, H., 2009. Chitosan-coated magnetic nanoparticles as carriers of 5-fluorouracil: preparation, characterization and cytotoxicity studies. Colloids Surf., B 68 (1), 1–6.

Zhuang, C., She, Y., Zhang, H., Song, M., Han, Y., Li, Y., Zhu, Y., 2018. Cytoprotective effect of deferiprone against aluminum chloride-induced oxidative stress and apoptosis in lymphocytes. Toxicol. Lett. 285, 132–138.

Zustiak, S.P., Dadhwal, S., Medina, C., Steczina, S., Chehreghanianzabi, Y., Ashraf, A., Asuri, P., 2016. Three-dimensional matrix stiffness and adhesive ligands affect cancer cell response to toxins. Biotechnol. Bioeng. 113 (2), 443–452.

Zykwinska, A., Tripon-Le Berre, L., Sinquin, C., Ropartz, D., Rogniaux, H., Colliec-Jouault, S., Delbarre-Ladrat, C., 2018. Enzymatic depolymerization of the GY785 exopolysaccharide produced by the deep-sea hydrothermal bacterium Alteromonas infernus: Structural study and enzyme activity assessment. Carbohydr. Polym. 188, 101–107.